DOI: 10.3901/CJME.2014.0929.155, available online at www.springerlink.com; www.cjmenet.com; www.cjmenet.com.cn

Atlas Based Kinematic Optimum Design of the Stewart Parallel Manipulator

SHAO Zhufeng[1, 2], TANG Xiaoqiang[1, 2, *], WANG Liping[1, 2], and SUN Dengfeng[3]

1 *State Key Laboratory of Tribology, Department of Mechanical Engineering, Tsinghua University, Beijing 100084, China*
2 *Beijing Key Lab of Precision/Ultra-precision Manufacturing Equipments and Control, Tsinghua University, Beijing 100084, China*
3 School of Aeronautics and Astronautics Engineering, Purdue University, West Lafayette, IN 47907, USA

Received March 6, 2014; revised September 23, 2014; accepted September 29, 2014

Abstract: Optimum design is a key approach to make full use of potential advantages of a parallel manipulator. The optimum design of multi-parameter parallel manipulators(more than three design parameters), such as Stewart manipulator, relies on analysis based and algorithm based optimum design methods, which fall to be accurate or intuitive. To solve this problem and achieve both accurate and intuition, atlas based optimum design of a general Stewart parallel manipulator is established, with rational selection of design parameters. Based on the defined spherical usable workspace(SUW), primary kinematic performance indices of the Stewart manipulator, involving workspace and condition number are introduced and analyzed. Then, corresponding performance atlases are drawn with the established non-dimensional design space, and impact of joint distribution angles on the manipulator performance is analyzed and illustrated. At last, an example on atlas based optimum design of the Stewart manipulator is accomplished to illustrate the optimum design process, considering the end-effector posture. Deduced atlases can be flexibly applied to both quantitative and qualitative analysis to get the desired optimal design for the Stewart manipulator with respect to related performance requirements. Besides, the established optimum design method can be further applied to other multi-parameter parallel manipulators.

Keywords: optimum design, performance atlas, parallel mechanism, Stewart

1 Introduction

Parallel manipulator is put forward with respect to the conventional serial manipulator, which possesses the significant structural feature of closed-loop chains. A parallel manipulator is composed of the base and the end effector, which are connected together by several identical limbs[1]. The base is usually fixed, while the end effector has multiple degrees of freedom. Generally, the number of independent actuators equals that of the manipulator's degrees of freedom, without considering actuation redundancy. Compared with serial manipulators, parallel manipulators possess evident advantages, e.g, large load-to-weight ratio, high accuracy, improved stiffness. Based on above merits, parallel manipulators have been widely applied in the industry field and also attracted great academic attention[2–3]. However, theories and technologies on parallel manipulators are still inadequate, which limit their potential in practical applications. As an important issue of both theoretical research and engineering application, optimum design is a great approach to improve the performance of parallel manipulators and will make parallel manipulators more attractive to the industry[4].

Optimum design of the parallel manipulator is always recognized as a challenging issue，and is mainly based on the kinematics now[5]. Many researchers have spent a lot of effort in this field that can be summarized into three categories: The first one can be named as the analysis based optimum design. Performance indices are analyzed one by one to accumulate rough design principles, and the dimension synthesis is carried out accordingly[6–7]. The second category is referred as the algorithm based optimum design, which starts with determining the exact target, based on single or multiple performance indices. Then, the optimum design issue is converted to a multi-objective optimization problem, and solved with complex nonlinear algorithms, such as genetic algorithms and artificial neural networks[8–9]. The last one is the atlas based optimum design. Based on drawn performance atlases, optimum parameters can be determined accurately and intuitionally[10–12]. The first method is simple to be carried out, but obtained design principles are inaccurate. Parameters with better performance can be deduced, while

* Corresponding author. E-mail: tang-xq@mail.tsinghua.edu.cn
Supported by National Natural Science Foundation of China(Grant Nos. 51205224, 51475252), and National Outstanding Youth Science Foundation of China(Grant No. 51225503)

the optimal result is hard to get, especially when there are contradictions among obtained principles. The second and the third methods are equivalent on deducing the optimal result. However, algorithm based optimum design fails to illustrate the relationship between design parameters and manipulator performances, and has to restart again when the target changes. Thus, atlas based optimum design is more advantageous. In addition, due to limitation on the number of design parameters, performance atlas based optimum design is only adopted by lower-mobility parallel manipulators with fewer design parameters now. In this paper, atlas based optimum design is carried out on a general 6 degree-of-freedoms(DOF) Stewart parallel manipulator for the first time, considering five design parameters, through proper parameter selection and sensible analysis.

In the process of optimal design, some typical kinematic indices are inevitablly adopted to evaluate the performance of the parallel manipulator. Workspace is the basic requirement of practical application. MERLET, et al[13], carried out the workspace analysis on the planar parallel manipulator, putting forward the constant orientation workspace, maximal workspace, and inclusive workspace. Then, the workspace of spatial parallel manipulators are studied, and workspaces of Stewart manipulators with different parameters are compared[14]. Further, workspace has been adopted as an important evaluation criterion for the optimum design of parallel manipulator[15–17]. The condition number of the kinematic Jacobian matrix is recognized as a comprehensive kinematic performance index and has been used by some researchers to carry out the optimum design. KLEIN, et al[18], discussed the local condition number and minimal singularity value of the kinematic Jacobian matrix on redundant manipulators. The condition number of the Jacobian matrix is also known as the dexterity of the parallel manipulator[19]. Later, the global conditioning index is introduced and used in the optimum design of the parallel manipulator[20–21]. The aforementioned indices are adopted in the following analysis, and corresponding atlases are deduced, which reveal the performance trend of the general Stewart manipulator.

Our study object, as shown in Fig. 1, is the 6 DOF Stewart parallel manipulator[22–24], consisting of two bodies (the base and the end effector) as well as six extensible limbs. Each limb is driven by a set of servomotor and ball screw. One end of the limb is connected to the base by a universal joint, while the other end is connected to the end effector by a spherical joint.

The reminder of this paper is organized as follows. In the next section, kinematics of the Stewart manipulator is analyzed and the Jacobian matrix is deduced. In section 3, the non-dimensional design space of the Stewart manipulator is established. Singularity and workspace of the Stewart platform are discussed in section 4, and workspace atlases are derived. Global conditioning index is discussed in section 5, and corresponding atlases are drawn. In section 6, an example on atlas based optimum design of the Stewart manipulator is given to show the implementation procedure. Finally, conclusions of this paper are given.

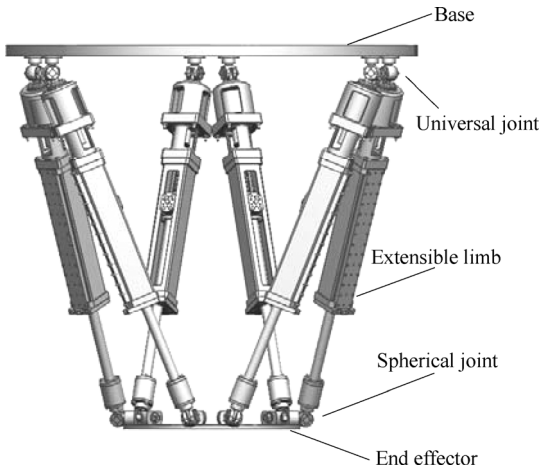

Fig. 1. Configuration of Stewart parallel manipulator

2 Kinematics Analysis

Fig. 2 illustrates the kinematic model of the Stewart manipulator. The base is defined by rotation centers of universal joints B_1, B_2, B_3, B_4, B_5, B_6, while the end effector is defined by rotation centers of spherical joints, marked with points P_1, P_2, P_3, P_4, P_5, P_6. The base frame $\{\mathbf{B}\}$:*O-XYZ* is located at the geometric center of the base, with the *X*-axis pointing at the midpoint of section B_1B_6, and the *Z*-axis is perpendicular to the base downward. The end-effector frame $\{\mathbf{P}\}$:*o-xyz* is attached to the geometric center of the end effector, with the *x*-axis pointing at the middle of section P_1P_6, and the *z*-axis perpendicular to the end effector downward. The end-effector position is described by the translation vector $\boldsymbol{t} = [x, y, z]^{\mathrm{T}}$, pointing from the origin of the base frame to the origin of the end-effector frame.

The Euler representation is adopted to describe the end-effector posture, namely, a rotation of angle θ about the *X*-axis, followed by a rotation of angle φ around the *Y*-axis, and finally followed by a rotation of angle ϕ around the *Z*-axis. Relative to the base frame, the rotation matrix of the end effector equals the product of three basic rotation matrices

$$\boldsymbol{R} = \boldsymbol{R}_3(Z,\phi)\boldsymbol{R}_2(Y,\varphi)\boldsymbol{R}_1(X,\theta) = \begin{pmatrix} \mathrm{c}\phi\mathrm{c}\varphi & \mathrm{c}\phi\mathrm{s}\varphi\mathrm{s}\theta - \mathrm{s}\phi\mathrm{c}\theta & \mathrm{c}\phi\mathrm{s}\varphi\mathrm{c}\theta + \mathrm{s}\phi\mathrm{s}\theta \\ \mathrm{s}\phi\mathrm{c}\varphi & \mathrm{s}\phi\mathrm{s}\varphi\mathrm{s}\theta + \mathrm{c}\phi\mathrm{c}\theta & \mathrm{s}\phi\mathrm{s}\varphi\mathrm{c}\theta - \mathrm{c}\phi\mathrm{s}\theta \\ -\mathrm{s}\varphi & \mathrm{c}\varphi\mathrm{s}\theta & \mathrm{c}\varphi\mathrm{c}\theta \end{pmatrix}, \tag{1}$$

where s and c symbols stand for sine and cosine operations, respectively.

The position vector of point P_i can be described in the base frame by the rotation matrix and translation vector as

$$\boldsymbol{P}_i = \boldsymbol{R}\boldsymbol{p}_i + \boldsymbol{t}\ ,\quad i = 1,2,\cdots,6, \tag{2}$$

where $\boldsymbol{p}_i$ is the position vector of point P_i under the end-effector frame.

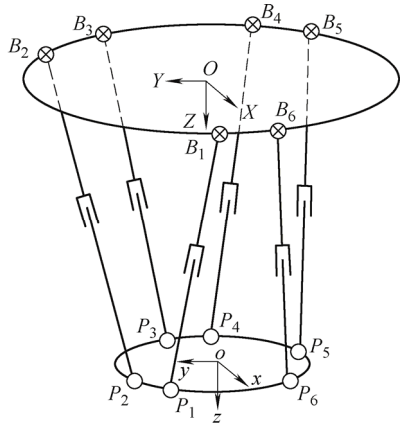

(a) Isometric view

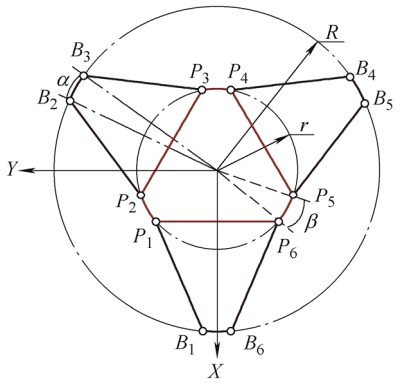

(b) Top view

Fig. 2. Kinematic model of the Stewart parallel manipulator

Next, the limb vector $\boldsymbol{S}_i$ (pointing from B_i point to P_i point) can be derived as

$$\boldsymbol{S}_i = \boldsymbol{P}_i - \boldsymbol{b}_i, \tag{3}$$

and $\boldsymbol{b}_i$ is the position vector of point B_i expressed in the base frame.

With the limb length

$$L_i = \|\boldsymbol{S}_i\|, \tag{4}$$

the unit limb vector can be obtained as

$$\boldsymbol{s}_i = \boldsymbol{S}_i / L_i\,. \tag{5}$$

Taking the derivative of Eq. (3) with respect to time yields the velocity expression as

$$\dot{\boldsymbol{S}}_i = \dot{\boldsymbol{t}} + \boldsymbol{\omega} \times (\boldsymbol{R}\boldsymbol{p}_i), \tag{6}$$

where $\boldsymbol{\omega}$ is the angular velocity of the end effector.

According to the physical meaning, $\dot{\boldsymbol{S}}_i$ can also be described with the sliding velocity $\dot{L}_i$ and the angular velocity $\boldsymbol{W}_i$ of the ith limb as

$$\dot{\boldsymbol{S}}_i = \dot{L}_i \boldsymbol{s}_i + L_i \boldsymbol{W}_i \times \boldsymbol{s}_i. \tag{7}$$

In order to deduce the Jacobian matrix, Eqs. (6) and (7) are considered together, which give

$$\dot{\boldsymbol{t}} + \boldsymbol{\omega} \times (\boldsymbol{R}\boldsymbol{p}_i) = L_i \boldsymbol{W}_i \times \boldsymbol{s}_i + \dot{L}_i \boldsymbol{s}_i. \tag{8}$$

Take the dot product of Eq. (8) with the unit limb vector $\boldsymbol{s}_i$ at both sides, and the velocity mapping equation can be established as

$$\boldsymbol{s}_i \bullet \dot{\boldsymbol{t}} + \left[(\boldsymbol{R}\boldsymbol{p}_i) \times \boldsymbol{s}_i\right] \bullet \boldsymbol{\omega} = \dot{L}_i.$$

The above equation can be organized in matrix form as

$$\boldsymbol{J}\dot{\boldsymbol{X}} = \dot{\boldsymbol{L}}, \tag{9}$$

where $\boldsymbol{J}$ is the Jacobian matrix of the Stewart manipulator, and can be expressed as

$$\boldsymbol{J} = \left[\boldsymbol{s}_1^{\mathrm{T}}, (\boldsymbol{R}\boldsymbol{p}_1 \times \boldsymbol{s}_1)^{\mathrm{T}}; \boldsymbol{s}_2^{\mathrm{T}}, (\boldsymbol{R}\boldsymbol{p}_2 \times \boldsymbol{s}_2)^{\mathrm{T}}; \cdots; \boldsymbol{s}_6^{\mathrm{T}}, (\boldsymbol{R}\boldsymbol{p}_6 \times \boldsymbol{s}_6)^{\mathrm{T}}\right]. \tag{10}$$

3 Design Space

The performance of the parallel manipulator depends on the end-effector pose as well as the architecture. After the telescopic proportion of the limb is determined, the architecture of the Stewart manipulator can be described with five geometric parameters(considering practical experience, the telescopic range of the extensible limb is given as from k to $2k$ here). Four parameters are illustrated in Fig. 2(b), namely, circumradius of the end effector r, circumradius of the base R, distribution angle of the spherical joint β, and distribution angle of the universal joint α. In order to describe the workspace center and measure the manipulator volume, the initial distance h between the base and the effector is chosen as the fifth geometric parameter, when each limb is of the initial length $1.5k$. Thus, three length parameters and two angle parameters are chosen to define the architecture of the Stewart manipulator.

Let's focus on length parameters first. Theoretically, each of these three parameters can take an arbitrary value from zero to infinity. And, their combinations are infinity. In order to illustrate all possible combinations within a finite area, length parameters must be normalized. Define a dimension factor as

$$\eta = (r + R + h)/3. \tag{11}$$

Then, we can get three dimensionless parameters as

$$l_1 = r/\eta, l_2 = R/\eta, l_3 = h/\eta, \tag{12}$$

where $l_1+l_2+l_3=3$. Length parameters can be illustrated in a

plane to facilitate performance description and analysis. As shown in Fig. 3, l_1-axis is established parallel to the Y-axis, l_2-axis and l_3-axis are mutually perpendicular, and the angle between l_1-axis and l_2-axis is $3\pi/4$. Each combination of these three parameters can also be expressed in the Cartesian coordinate system, with the relationship as

$$\begin{cases} x = \sqrt{2}l_3 + l_1/\sqrt{2}, \\ y = l_1. \end{cases}$$

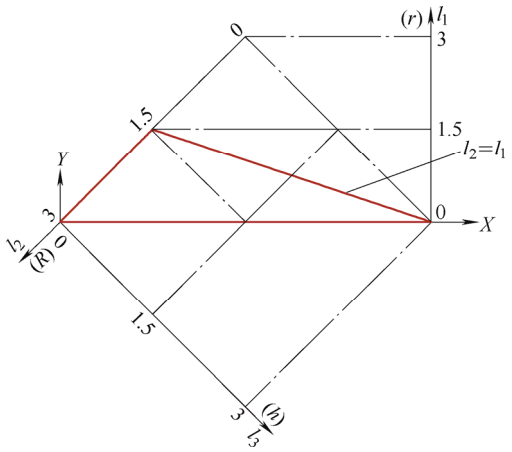

Fig. 3. Design space of length parameters

The end-effector circumradius r should not be greater than the base circumradius R, namely, $l_2 \geqslant l_1$. Then, the design space of length parameters is determined as shown in Fig. 3(enclosed by red lines).

Theoretically, range of angle parameters(joint distribution angles) is from zero to sixty degrees. Considering the joint installation space, the available range is narrowed, and is between five and sixty degrees. Further discussion on the angle range is carried out in the next section.

4 Workspace Analysis and Workspace Atlases

The reachable workspace of the Stewart manipulator, which is encircled by twelve envelope surfaces, has an irregular shape with the singular loci inside. Thus, regular usable workspace(RUW) is defined here as the regular-shaped maximum continuous workspace without a singularity. Since the Stewart manipulator is a circular symmetric structure, the spherical usable workspace(SUW) is adopted in this paper, which is the maximum continuous spherical workspace with no singular locus inside. In most cases, the SUW of the Stewart manipulator is the maximum inscribed sphere of the reachable workspace. In the following analysis, the zero-rotation SUW is considered at first, when rotation angles of the end effector are zero.

4.1 Singularity

In order to determine the SUW, singularities of the Stewart manipulator are discussed. As shown in Eq. (9), it is obvious that there exists only the second type singularity[25] for the Stewart manipulator, when $\det(\boldsymbol{J}) = 0$. Such singularities of the Stewart manipulator can be further divided into three categories, such as architecture singularity, configuration singularity and formulation singularity. If the base and the end effector of the Stewart manipulator are similar polygons, the architecture singularity occurs, which should be completely avoided in the design. When the base and the end effector coincide, or limbs are of the same length with the end-effector rotation of $\pm\pi/2$ around the Z-axis, the configuration singularity appears. The formulation singularity is usually introduced by the adopted description method of the end effector posture. In this paper, since the Euler representation is used, this type of singularity happens only when the rotation angle around the Y-axis is $\pm\pi/2$ [26–27].

The architecture singularity can be avoided by the rational definition of base and end-effector frames. As shown in Fig. 2(b), base and end-effector frames are established with a deviation angle of $\pi/3$ relative to the joint distribution. And, only when $\alpha = \beta = \pi/3$, the architecture singularity appears. Thus, available ranges of angle parameters α and β should be further narrowed, and is between 5° and 55°. At the same time, the rotation angle of $\pm\pi/2$ is too large to be available for the Stewart manipulator. Thus, only the configuration singularity, where the base and the end effector coincide, needs to be paid attention to in the follow-up workspace analysis.

4.2 Workspace atlases

With given joint distribution angles($\alpha = \beta = 10^\circ$), the zero-rotation SUW atlas can be derived, considering length parameters, as shown in Fig. 4. The radiuses of both maximum inscribed sphere and the SUW is obtained through numerical simulation with the MATLAB software. From the results, we can conclude the following.

(1) The design space can be divided into three regions by two lines, namely $l_2 = l_3 + 1.5$, and $l_2 = 1.5$.

(2) In the left region, the SUW is different from the maximum inscribed sphere of the reachable workspace, and the SUW radius is generally proportional to h.

(3) In the middle region, the SUW radius increase with the decrease of r in general.

(4) In the right region, if l_2 is specified, the radius of SUW grows with the increase of l_3 and the decrease of l_1.

(5) The maximum SUW radius appears at lower right and the bottom area of line $l_2 = l_3 + 1.5$.

Then, let's discuss the impact of joint distribution angles on the SUW radius of the Stewart manipulator. Firstly, three groups of l_1, l_2, and l_3 are selected to estimate the relationship between radius of the zero-rotation SUW and joint distribution angles. As shown in Fig. 5, it indicates that the SUW radius increases with the decrease of the angle sum $\alpha + \beta$, and the radius will not change for different values of α and β, when their sum $\alpha + \beta$ is constant.

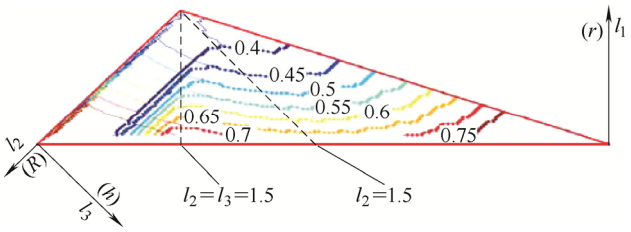

Fig. 4.　Workspace atlas under zero-rotation condition

Solid: maximum inscribed sphere of the reachable workspace
Dashed: SUW

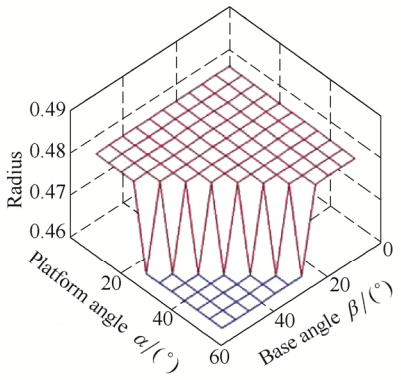

(a) l_1=0.6, l_2=2, l_3=0.4

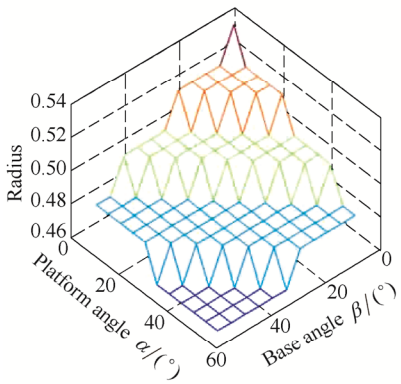

(b) l_1=0.5, l_2=1.5, l_3=1

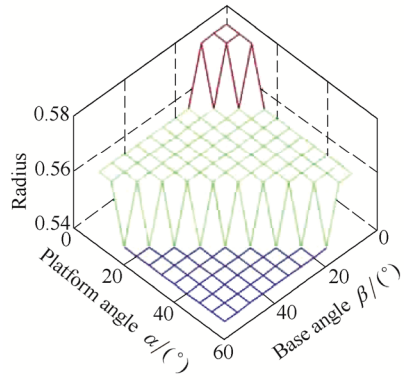

(c) l_1=0.5, l_2=0.9, l_3=1.6

Fig. 5.　Relationship between the SUW radius and joint distribution angles

Further, joint distribution angles are analyzed through superimposing on the design space of length parameters to confirm their influences on workspace, as shown in Fig. 6. In Fig. 6(a), solid lines show the SUW atlas for $\alpha=\beta=30^\circ$, while dashed lines illustrate the workspace atlas for $\alpha=\beta=50^\circ$. In Fig. 6(b), solid curves show the workspace atlas for $\alpha=55^\circ,\beta=5^\circ$, while dashed curves reveal the workspace atlas for $\alpha=5^\circ,\beta=55^\circ$. From these atlases, we can tell the following.

(1) In the left region, the SUW radius is mainly determined by the singularity condition. Impact of joint distribution angles cannot be reflected obviously.

(2) In the middle and the right regions, the SUW radius is affected by the sum of joint distribution angles, and the impact of joint distribution angles on the radius is more obvious when l_1 is larger.

(3) In the middle and the right regions, when the sum of joint distribution angles is fixed, specific values of α and β have little impact on the SUW radius.

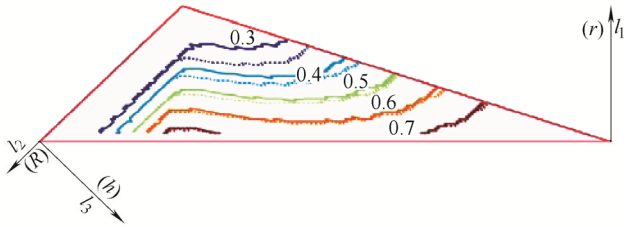

(a) Dashed: $\alpha=\beta=50^\circ$; solid: $\alpha=\beta=30^\circ$

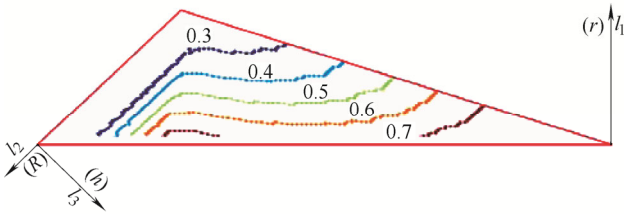

(b) Dashed: $\alpha=5^\circ$, $\beta=55^\circ$; solid: $\alpha=55^\circ$, $\beta=5^\circ$

Fig. 6.　SUW atlases considering different joint distribution angles

Above laws can be explained by the expression for the telescopic length of the limb, which is

$$L_{\text{init}}^2=(3k/2)^2=h^2+R^2+r^2-2Rr\cos\left[\pi/3-(\alpha+\beta)/2\right], \tag{13}$$

where k is the minimum length of the limb, and equals the telescopic length. When the sum of joint distribution angles $(\alpha+\beta)$ increases, the telescopic length is reduced. The reachable workspace of the Stewart manipulator is mainly determined by the telescopic length of the limb. Thus, the reachable workspace and its inscribed sphere(SUW in the middle and right regions) shrink. In addition, if h is fixed, an increase of r will enlarge the proportion of Rr to $h^2+R^2+r^2$ in Eq. (13), and makes the impact of joint distribution angles obvious.

In all, in order to obtain a large SUW, sum of joint distribution angles should be reduced, and Stewart manipulators with large h or large difference between R and r have advantages.

5 Atlases of Global Conditioning Index

In mathematics, the condition number is used to analyze sensitivity and uncertainty of the solution of linear equations. When adopted in the parallel manipulator, the condition number of the Jacobian matrix is an important local performance index, which indicates dexterity and isotropy, as well as implies velocity, accuracy and rigid features. The condition number of the Jacobian matrix can be expressed as

$$\kappa = \sigma_{\max} / \sigma_{\min}, \tag{14}$$

where $\sigma_{\max}$ and $\sigma_{\min}$ are maximum and minimum singular values of the Jacobian matrix, and $1 \leqslant \kappa \leqslant \infty$.

The local conditioning index(LCI) is defined as the reciprocal of the condition number of the Jacobian matrix. In order to evaluate the performance change of a parallel manipulator with different design parameters, the Global Conditioning Index (GCI) is adopted, which can be expressed as

$$\Gamma_\kappa = \int_W \frac{1}{\kappa} \mathrm{d}W \Big/ \int_W \mathrm{d}W, \tag{15}$$

where W is the regular usable workspace of the parallel manipulator. A larger GCI value promises a better control accuracy in general.

The Stewart parallel manipulator possesses six degrees of freedom in the terminal Cartesian coordinate system, including three rotational degrees of freedom and three translational degrees of freedom. Considering the dimensional homogeneity, the Jacobian matrix of the Stewart manipulator is normalized, using the end-effector circumradius r. And, the normalized Jacobian matrix can be written as

$$\boldsymbol{J}_{\mathrm{N}} = \left[\boldsymbol{s}_1^{\mathrm{T}}, \left(\boldsymbol{R} \frac{\boldsymbol{p}_1}{r} \times \boldsymbol{s}_1 \right)^{\mathrm{T}}; \boldsymbol{s}_2^{\mathrm{T}}, \left(\boldsymbol{R} \frac{\boldsymbol{p}_2}{r} \times \boldsymbol{s}_2 \right)^{\mathrm{T}}; \cdots; \boldsymbol{s}_6^{\mathrm{T}}, \left(\boldsymbol{R} \frac{\boldsymbol{p}_6}{r} \times \boldsymbol{s}_6 \right)^{\mathrm{T}} \right].$$

Then, the velocity mapping function of the Stewart manipulator can be expressed as

$$\boldsymbol{J}_{\mathrm{N}} \begin{pmatrix} \dot{\boldsymbol{t}} \\ r\boldsymbol{\omega} \end{pmatrix} = \boldsymbol{J}_{\mathrm{N}} \dot{\boldsymbol{X}}_{\mathrm{N}} = \dot{\boldsymbol{L}}.$$

Based on the Jacobian matrix obtained above, corresponding GCI atlas can be drawn, as shown in Fig. 7 ($\alpha = \beta = 10^\circ$, zero-rotation SUW). We can conclude the following.

(1) Larger values are in the center area, while minimum values lie in left and right ends.

(2) In the left area, for a given l_1, GCI value grows with the decrease of l_2 and the increase of l_3.

(3) In the right area, when l_1 is determined, GCI value grows with the decrease of l_3 and the increase of l_2.

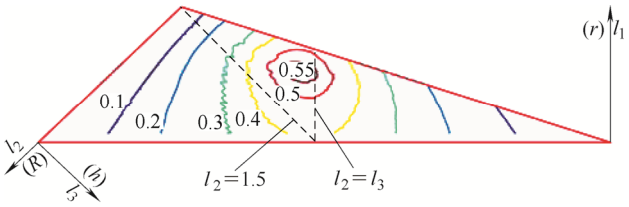

Fig. 7. GCI atlas

In Fig. 8, the impact of joint distribution angles α and β on the GCI value is analyzed for three sets of length parameters. Obviously, the GCI value decreases with the increase of the sum of joint distribution angles. However, when their sum is fixed, separate joint distribution angles have little effect on the GCI value.

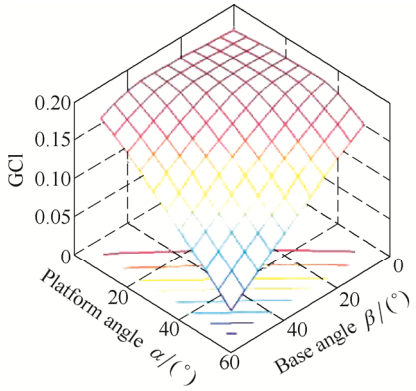

(a) l_1=0.6, l_2=2, l_3=0.4

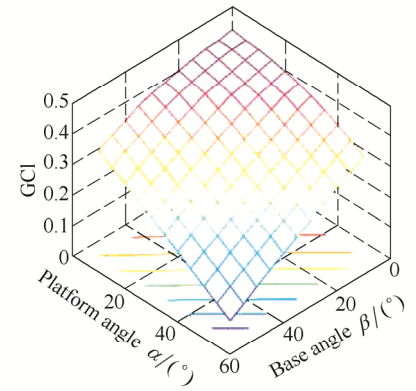

(b) l_1=0.5, l_2=1.5, l_3=1

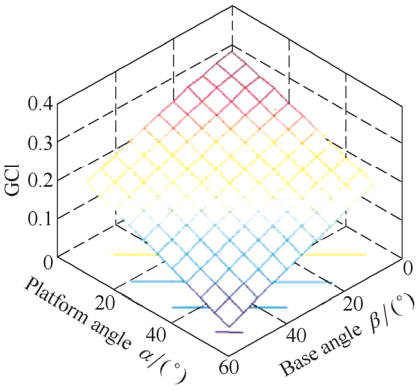

(c) l_1=0.5, l_2=0.9, l_3=1.6

Fig. 8. Relationship between the GCI value and joint distribution angles

The influence of joint distribution angles can also be deduced from GCI atlases considering different joint distribution angles, as shown in Fig. 9. In Fig. 9(a), dashed curves illustrate the GCI atlas for $\alpha=\beta=50^\circ$, while solid curves correspond to that for $\alpha=\beta=30^\circ$. In Fig. 9(b), dashed curves show the GCI atlas for $\alpha=5^\circ$ and $\beta=55^\circ$, while solid curves represent that for $\alpha=55^\circ$ and $\beta=5^\circ$, i.e., the sum of joint distribution angles is a constant value of 60°. Comparative analysis of these curves indicates the following.

(1) Sum of joint distribution angles has obvious impact on the GCI atlas. However, specific values of α and β have little influence, if their sum is invariant.

(2) When sum of joint distribution angles($\alpha+\beta$) increases, the region with large GCI value shrinks, and moves toward the upper left in the design space.

(3) In most area of the design space, the GCI value decreases, when the sum of joint distribution angles $\alpha+\beta$ grows. Only in a small area surrounded by lines l_2=1.5 and l_2=l_3, the GCI value may increase with growing angle sum.

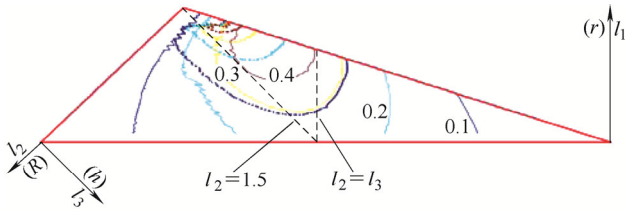

(a) Dashed: α=β=50°; solid: α=β=30°

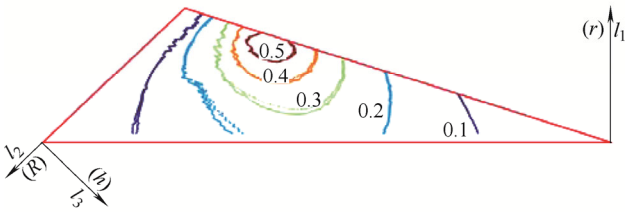

(b) Dashed: α=5°, β=55°; solid: α=55°, β=5°

Fig. 9.　GCI atlases considering different joint distribution angles

6　Example of Atlas Based Optimum Design

The first step of atlas based optimum design for the Stewart manipulator is to determine joint distribution angles and telescopic proportion of the limb. Based on above analysis, we can conclude that joint distribution angles impact the manipulator performance mainly in the form of their sum, and smaller sum is indicative of a better kinematic performance. Thus, the sum of joint distribution angles should be as small as possible, on the condition of meeting the installation requirement of spherical and universal joints. In detailed design phase, specific values of joint distribution angles can be adjusted more precisely with little impact on manipulator performances. In this section, the sum of joint distribution angles is set to 20° ($\alpha+\beta=20^\circ$), in order to make full use of obtained atlases. The telescopic range of the limb can be determined according to engineering experience. Here, the maximum length of the limb is assumed twice the minimum length.

The next step is to establish the design space and draw required performance atlases. Since this part has been completed, we can move on to the third step to obtain a candidate region in the design space. If the radius of the zero-rotation SUW is supposed to be not less than 0.45 and GCI value is larger than or equal to 0.5(performance requirements), the candidate region can be determined, as shown in Fig. 10. And, candidate ranges of length parameters described in the design space can be obtained approximately as

$$l_1\subset[0.44,0.71],\ l_2\subset[1.13,1.52],\text{ and }\ l_3\subset[0.81,1.21].$$

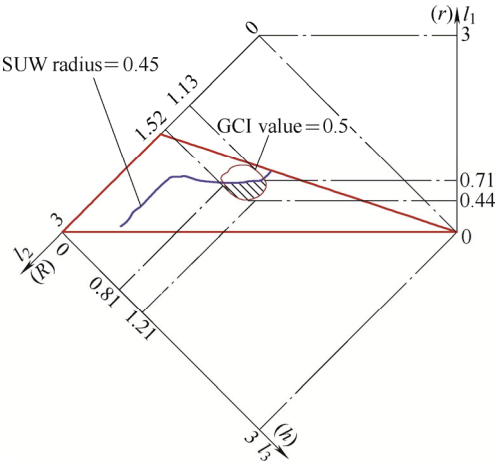

Fig. 10.　Candidate region of the optimum design

In the fourth step, a set of non-dimensional optimum parameters can be determined by the most desired performance within the obtained candidate region. If we want to get a manipulator with maximum workspace in the candidate region, according to Figs. 4 and 10, the lowest point in the candidate region should be adopted. Thus, the minimum value of l_1 is adopted, and l_1=0.44, l_2=1.36 and l_3=1.20. Of course, the maximum GCI value can also be adopted as the target to get another set of optimum parameters.

In the fifth step, the dimension factor η is determined, which converts the non-dimensional parameters into practical dimensional ones. The Stewart manipulator is usually adopted to implement the 5-axis machine tool. Thus, the yaw angle, the angle between the end effector and the horizontal plane, is used here to describe the end-effector posture. The LCI is adopted to give more refined description of the manipulator performance. As shown in Fig. 11, if the LCI is supposed to be not less than 0.4, the radius of SUW can be determined, such as 0.29, 0.38, 0.46 and 0.53, depending on the yaw angle requirement. The SUW radius of the dimensional manipulator equals the product of dimension factor and the non-dimensional SUW radius. For example, if the desired SUW radius is 400mm, the factor η can be calculated as

$$\eta_1 = 0.4/0.29 = 1.38 \text{ m}, \quad \eta_2 = 0.4/0.38 = 1.05 \text{ m},$$
$$\eta_3 = 0.4/0.46 = 0.87 \text{ m},$$

corresponding to yaw angle requirements of 15°, 10° and 5°, respectively.

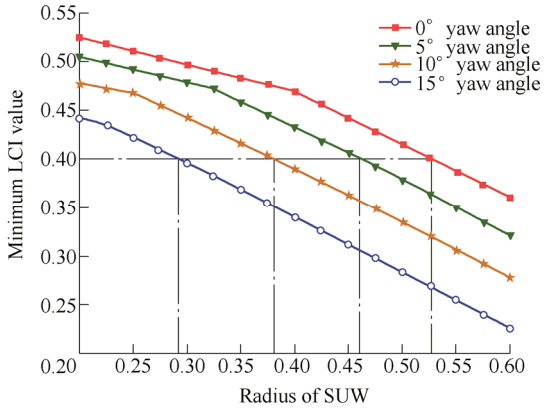

Fig. 11. Radius of SUW considering end-effector posture

The last step is to calculate the dimensional parameters. The dimensional parameters of the optimum Stewart manipulator can be determined with the obtained dimension factor and non-dimension parameters. Taking η_2 for example, we can get practical parameters from Eq. (12) as

$$r = l_1 \times \eta_2 = 0.46 \text{ m}, \quad R = l_2 \times \eta_2 = 1.43 \text{ m},$$
$$h = l_3 \times \eta_2 = 1.26 \text{ m}.$$

Together with the joint distribution angles, location of spherical and universal joints can be determined. Then, with the telescopic proportion, initial length and telescopic range of the limb can be figured out.

7 Conclusions

(1) The spherical usable workspace is defined to describe the workspace of the Stewart manipulator, and establishes the basis for global index analysis.

(2) When the telescopic range of the extensible limb is given, the design parameters of the general Stewart manipulator is rationally simplified into two angle and three length design parameters, namely, initial distance, joint distribution angles and radiuses of both the base and the end effector. The dimensionless design space of length parameters is established in the two-dimensional plane.

(3) Primary kinematic indices such as workspace and condition number have been discussed, joint distribution angles are analyzed through superimposing on the design space of length parameters, and corresponding atlases are deduced. These atlases accurately illustrate variation trends of the manipulator performance in the finite non-dimensional design space with respect to parameter changes of the Stewart manipulator, and can be flexibly applied to quantitative and qualitative analysis to get the desired optimal design.

(4) Impact of joint distribution angles on kinematic performances is analyzed, which shows that the sum of joint distribution angles affects manipulator performances significantly. Generally, the Stewart manipulator with minor sum of joint distribution angles promises better kinematic performances with respect to workspace, isotropy and accuracy. At the same time, it is found that the Stewart manipulator with a large initial distance or large circumradius difference between the base and the end effector has an advantage on obtaining a large workspace.

(5) Atlas based kinematic optimum design of the Stewart parallel manipulator is established, and the proposed optimum method is well illustrated with an example, considering the end-effector posture. The established optimum design method can be further applied to other multi-parameter parallel manipulators.

References

[1] TANG X, TANG L, WANG J, et al. Workspace quality analysis and application for a completely restrained 3-DOF planar cable-driven parallel manipulator[J]. *Journal of Mechanical Science and Technology*, 2013, 27(8): 2391–2399.

[2] HOSTENS I, ANTHONIS J, RAMON H. New design for a 6 DOF vibration simulator with improved reliability and performance[J]. *Mechanical Systems and Signal Processing*, 2005, 19(1): 105–122.

[3] LI B, CAO Y, ZHANG Q, et al. Orientation-singularity representation and orientation-capability computation of a special class of the Gough-Stewart parallel mechanisms using unit quaternion[J]. *Chinese Journal of Mechanical Engineering*, 25(6): 1096–1104.

[4] STAICU S, ZHANG D. Dynamic modeling of a 4-DOF parallel kinematic machine with revolute actuators[J]. *International Journal Manufacturing Research*, 2008, 3(2): 172–187.

[5] LIU X J, WANG J, ZHENG H J. Optimum design of the 5R symmetrical parallel manipulator with a surrounded and good-condition workspace[J]. *Robotics and Autonomous Systems*, 2006, 54(3): 221–233.

[6] YAO R, TANG X, WANG J, et al. Dimension optimization design of the four-cable driven parallel manipulator in FAST[J]. *IEEE/ASME Transactions on Mechatronics*, 2010, 15(6): 932–941.

[7] TANG X, YAO R. Dimensional design on the six-cable driven parallel manipulator of FAST[J]. *Journal of Mechanical Design*, 2011, 11: 1–12.

[8] CECCARELLI M, LANNI C. A multi-objective optimum design of general 3R manipulators for prescribed workspace limits[J]. *Mechanism and Machine Theory*, 2004, 39(2): 119–132.

[9] GAO Z, ZHANG D, GE Y. Design optimization of a spatial six degree-of-freedom parallel manipulator based on artificial intelligence approaches[J]. *Robotics and Computer-Integrated Manufacturing*, 2010, 26(2): 180–189.

[10] WANG B, HAN W. Performance atlases of global conditioning index of planar 3-DOF parallel manipulator with accuracy redundancy[J]. *Advanced Materials Research*, 2012, 479–481: 2316–2320.

[11] LIU X J, WANG J, PRITSCHOW G. Performance atlases and optimum design of planar 5R symmetrical parallel mechanisms[J]. *Mechanism and Machine Theory*, 2006, 41(2): 119–144.

[12] GAO F, ZHANG X, ZHAO Y, et al. A physical model of the solution space and the atlases of the reachable workspaces for 2-DOF parallel plane wrists[J]. *Mechanism and Machine Theory*, 1996, 31(2): 173–184.

[13] MERLET J P, GOSSELIN C M, MOULY N. Workspaces of planar parallel manipulators[J]. *Mechanism and Machine Theory*, 1998, 33(1, 2): 7–20.
[14] MERLET J P. Determination of 6D workspaces of Gough-type parallel manipulator and comparison between different geometries[J]. *International Journal of Robotics Research*, 1999, 18(9): 902–916.
[15] MERLET J P. Designing a parallel manipulator for a specific workspace[J]. *International Journal of Robotics Research*, 1997, 16(4): 545–556.
[16] HAY A M, SNYMAN J A. Methodologies for the optimal design of parallel manipulators[J]. *International Journal for Numerical Methods in Engineering*, 2004, 59 (3): 131–152.
[17] BAI S. Optimum design of spherical parallel manipulators for a prescribed workspace[J]. *Mechanism and Machine Theory*, 2010, 45(2): 200–211.
[18] KLEIN C A, BLAHO B E. Dexterity measures for the design and control of kinematically redundant manipulator[J]. *International Journal of Robotics Research*, 1997, 6(2): 72–83.
[19] SALISBURY J K, GRAIG J J. Articulated hands: force control and kinematic issues[J]. *International Journal of Robotics Research*, 1982, 1(1): 4–17.
[20] LIU X J, JIN Z L, GAO F. Optimum design of 3-DOF spherical parallel manipulators with respect to the conditioning and stiffness indices[J]. *Mechanism and Machine Theory*, 2000, 35(9): 1257–1267.
[21] GAO F, LIU X J, GRUVER W A. Performance evaluation of two degree-of-freedom planar parallel robots[J]. *Mechanism and Machine Theory*, 1998, 33(6): 661–668.
[22] TANG X, SHAO Z. Trajectory planning and tracking control of a multi-level hybrid support manipulator in FAST[J]. *Mechatronics*, 2013, 23(8): 1113–1122.
[23] YAO R, ZHU W, HUANG P. Accuracy analysis of Stewart platform based on interval analysis method[J]. *Chinese Journal of Mechanical Engineering*, 2013, 26(1): 29–34.
[24] SHAO Z, TANG X, CHEN X, et al. Research on the inertia matching of the Stewart parallel manipulator[J]. *Robotics and Computer-Integrated Manufacturing*, 2012, 28(6): 649–659.
[25] GOSSELIN C, ANGELES J. Singularity analysis of closed-loop kinematic chains[J]. *IEEE Transaction on Robotics and Automation*, 1990, 6(3): 281–290.
[26] MA O, ANGELS J. Architecture singularities of platform manipulators[C]// *Proceedings of the IEEE International Conference on Robotics and Automation*, Sacramento, California, USA, April, 9–11, 1991: 1542–1547.
[27] MA J, HUANG Q, XIONG H, et al. Analysis and application of the singularity locus of the Stewart platform[J]. *Chinese Journal of Mechanical Engineering*, 2011, 24(1): 133–140.

Biographical notes

SHAO Zhufeng, born in 1983, is currently an assistant professor at *Department of Mechanical Engineering, Tsinghua University, China.* He received his PhD degree from *Tsinghua University, China*, in 2011. His research interests include design, dynamic analysis and control of the parallel manipulator.
Tel: +86-10-62794598-11; E-mail: shaozf@mail.tsinghua.edu.cn

TANG Xiaoqiang, born in 1973, is currently an associate professor and a PhD candidate supervisor at *Department of Mechanical Engineering, Tsinghua University, China.* His main research interests include parallel manipulator, cable robots, and motion control.
E-mail: tang-xq@mail.tsinghua.edu.cn

WANG Liping, born in 1967, is currently a professor and a PhD candidate supervisor at *Department of Mechanical Engineering, Tsinghua University, China.* His main research interests lie in the advanced manufacturing equipment.
E-mail: lpwang@mail.tsinghua.edu.cn

SUN Dengfeng, born in 1975, is currently an associate professor at *School of Aeronautics and Astronautics Engineering, Purdue University, USA*. His main research interests include modeling, simulation and optimization of large scale networked systems.
E-mail: dsun@purdue.edu